PCCP

PAPER

View Article Online
View Journal | View Issue

Cite this: *Phys. Chem. Chem. Phys.*, 2015, **17**, 28162

Role of the nanocrystallinity on the chemical ordering of Co_xPt_{100-x} nanocrystals synthesized by wet chemistry

Farid Kameche,[ab] Anh-Tu Ngo,[ab] Caroline Salzemann,[ab] Marco Cordeiro,[c] Eli Sutter[c] and Christophe Petit*[ab]

Received 20th February 2015,
Accepted 17th March 2015

DOI: 10.1039/c5cp01062d

www.rsc.org/pccp

Co_xPt_{100-x} nanoalloys have been synthesized by two different chemical processes either at high or at low temperature. Their physical properties and the order/disorder phase transition induced by annealing have been investigated depending on the route of synthesis. It is demonstrated that the chemical synthesis at high temperature allows stabilization of the fcc structure of the native nanoalloys while the soft chemical approach yields mainly poly or non crystalline structure. As a result the approach of the order/disorder phase transition is strongly modified as observed by high-resolution transmission electron microscopy (HR-TEM) studies performed during *in situ* annealing of the different nanoalloys. The control of the nanocrystallinity leads to significant decrease in the chemical ordering temperature as the ordered structure is observed at temperatures as low as 420 °C. This in turn preserves the individual nanocrystals and prevents their coalescence usually observed during the annealing necessary for the transition to an ordered phase.

A. Introduction

Metallic nanoalloys will initiate important development in nanotechnologies due to their specific chemical and physical properties (*i.e.* in catalysis, magnetism, optics, *etc.*).[1,2] It is now well known that these properties are mainly controlled by the fine tuning of structural parameters such as the size, the bimetallic composition and segregation processes.[3] Concerning their fabrication, the bottom up approach, either physical or chemical, is ideal to design this specific class of nanomaterials due to its versatility, facility and low cost. However, the realization of well-controlled bimetallic nanoparticles is not always straightforward from the know-how developed for monometallic nanoparticles.

In a sustainable approach, wet chemistry is well adapted to produce such nanoalloys in large amounts.[4] However at the nanometer scale, as the properties are strongly dependent on the size and the surface state (raw or passivated), it is crucial to develop methods where the crystallinity, the polydispersity in size and composition are finely controlled. Furthermore, despite the large amount of work made on the synthesis of nanoalloys by the chemical way,[1,2] there are still open questions considering the control of composition and especially the segregation process. For example, in chemical approaches, bimetallic nanoparticles are always passivated by an organic molecule and mainly obtained in a disordered A_1 phase where both metals are randomly dispersed in the crystalline lattice (Fig. 1A).

Among the nanoalloys, magnetic nanocrystals (NCs) are promising materials due to their strong potential in the development of applications especially for high-density data storage.[5–8] In this last domain, bimetallic alloys such as CoPt, FePt or CoRh represent a particularly interesting class of materials for the improvement of the recording on magnetic storage systems. Indeed, alloys such as CoPt (or FePt) have an ordered crystalline phase ($L1_0$) around the equi-atomic composition, which is intrinsic to the tetragonal symmetry (fct) of the crystal structure (Fig. 1C) and an ordered fcc structure ($L1_2$) for compositions around Co_3Pt or $CoPt_3$ (Fig. 1B).[9,10] The ordered $L1_0$ phase of the CoPt system is of particular interest thanks to its high coercivity (10 kOe) and the high magnetocrystalline anisotropy (4.9×10^6 J m^{-3}). In fact, CoPt NCs in the $L1_0$ phase have large uniaxial magnetic anisotropy energy and thus have the potential to exceed the superparamagnetic limit.[11,12] Moreover, these CoPt magnetic NCs are monodomain magnetic particles for a typical size below 10 nm.[13] Beyond this typical size, the NCs become polydomain magnetic and this leads to domain wall formation.[14] In the case of $CoPt_3$, the $L1_2$ phase presents

[a] *Sorbonne Universités, UPMC Univ Paris 06, UMR 8233, MONARIS, 4 place Jussieu, F-75005, Paris, France. E-mail: christophe.petit@upmc.fr*
[b] *CNRS, UMR 8233, MONARIS, 4 place Jussieu, F-75005, Paris, France*
[c] *Center for Functional Nanomaterials, Brookhaven National Laboratory, Upton, NY 11973, USA*

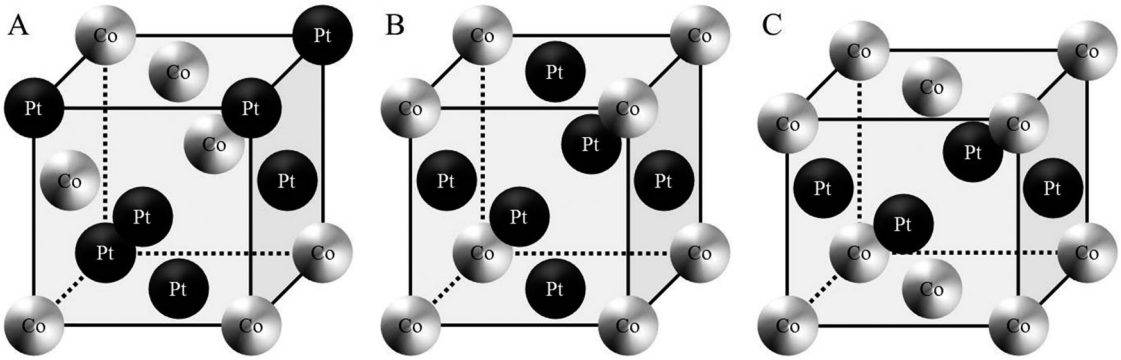

Fig. 1 Representation of Co_xPt_{100-x} structure in three different phases: (A) disordered phase A1 with cubic symmetry (B) ordered phase $L1_2$ with cubic symmetry (X = 25) and (C) ordered phase $L1_0$ with face centered tetragonal symmetry (X = 50).

also a very high magnetocrystalline anisotropy (2×10^6 J m^{-3}). Therefore, high control of both the chemical composition and size of the NCs alloy is essential for optimizing the magnetic nanoscale behavior.

Using the colloidal route, the CoPt's synthesis leads to the formation of NCs with the A_1 disordered structure. A thermal annealing is required to induce ordering toward $L1_0$ or $L1_2$ structure, depending on the composition.[15] For supported nanoparticles, the thermal assistances at high temperature (>300 °C) can lead to coalescence and sintering effects, which increase the size, modify the shape and destroy their organization.[15,16] Indeed, the driving force for coalescence and the change of shape is the minimization of surface energy by elimination of interfaces and appearance of grain boundaries and defects.[15] Thus, the elaboration of well-defined nanoparticles in the $L1_0$ or $L1_2$ ordered phase remains very difficult. We report here a new approach for the synthesis of Co_xPt_{100-x} nanoalloys allowing control of the nanocrystallinity and as a consequence of the order/disorder phase transition of the bimetallic CoPt NCs. The enhanced crystallinity allows decrease the transition temperature and so to minimize the coalescence effect usually reported during the annealing process. This is demonstrated by comparing the evolution of same nanoalloys obtained by wet chemistry either at high or at low temperature.

B. Experimental method

B-1 Chemicals

Cobalt(II) chloride hexahydrate ($CoCl_2{\cdot}6H_2O$) was from VWR. Platinum(II) acetylacetonate ($Pt(acac)_2$, 98%), oleylamine (80–90%) and sodium borohydride ($NaBH_4$, 99%) were from Acros. Sodium oleate (97%) and 1,2 hexadecanediol (98%) were from TCI. Oleic acid (90%), 1-octadecene (90%) platinum(IV) chloride ($PtCl_4$, 99.9%), octylamine (99%) and tetrakis(decyl)ammonium bromide (TDAB, 99%) were from Aldrich.

B-2 Apparatus

A JEOL (100 kV) model JEM-1011 transmission electron microscope (TEM) was used to determine the size of CoPt NCs. The average compositions of the nanocrystals are determined by energy dispersive spectrometry (EDS) analysis using a scanning electron microscope (SEM, JEOL 5510 LV) with IXRF Systems 500 digital processing. This has been done on a micrometric thick film made by slow evaporation of a concentrated solution of NCs on a silicon substrate at room temperature. The analysis is made on different parts of the sample. Magnetic measurements have been obtained by using a vibrating sample magnetometer (VSM) operating in a Quantum Design PPMS.

B-3 *In situ* transmission electron microscopy study

Variable temperature *in situ* experiments were performed in a JEOL 2100F field emission transmission electron microscope operated at 200 kV, equipped with a Gatan 652 high-temperature sample holder. The CoPt nanoparticles synthesized by two different methods were cast dropped on 3–5 layer thick graphene substrates supported on standard nickel grids. Graphene is used as support for two reasons: (i) it is very thin (<1 nm) and allows the HRTEM imaging of small nanoparticles and atom clusters. (ii) It is relatively stable during annealing to high temperatures. It gives the advantage of less rearrangement and redistribution of carbon from the support upon heating compared to amorphous carbon supports. The so-prepared TEM samples were loaded in the holder and annealed in vacuum in the temperature range between room temperature and 700 °C at pressure below 2×10^{-7} Torr. The annealing experiments were carried out step-wise: the temperature between steps was increased at the rate of 20 °C min^{-1}. Once the temperature of interest was reached the nanoparticles were stabilized for $\sim$30 minutes without exposure to the electron beam. Electron irradiation during imaging was kept intentionally low below 2 A cm^{-2} to prevent any uncontrolled electron beam induced structural changes.

B-4 Synthesis of CoPt nanoalloys by the polyol process

There is numerous synthesis of CoPt by the polyol process using mainly acetylacetonate derivatives for both cobalt and platinum.[17] However, they are quite complex, as the procedure requires different steps and always injection of the precursor at high temperature. Here in an attempt to control the crystallinity, a novel easy synthesis of CoPt nanoalloys by the so-called polyol process is achieved by mixing platinum(II) acetylacetonate

$(Pt(acac)_2)$ and homemade cobalt(II)oleate $(Co(oleate)_2)$. The choice of oleate derivate is driven by the fact that above 100 °C, $Pt(acac)_2$ reacts with oleic acid to form stable complexes such as $Pt(oleate)_2$.[18] We use $Co(oleate)_2$ as precursor because in the chemical synthesis of nanoalloys, it is important to use precursor having similar chemical structure in order to control the composition.[19] It is important to note that $Pt(oleate)_2$ is not available commercially and very difficult to synthesize. Conversely $Co(oleate)_2$ could be easily synthesized. The synthesis of the cobalt–oleate complex is adapted from the one of $Fe(oleate)_3$.[20] It is prepared by mixing cobalt(II) chloride hexahydrate (30 mmol in 30 ml of ultrapure water) and sodium oleate (60 mmol in a mixture of 40 ml of ethanol and 70 ml of hexane). The mixture is refluxed at 66 °C for 4 h and the organic phase is washed three times with ultrapure water in a separatory funnel. The remaining hexane in the organic phase is evaporated under vacuum in a rotavapor at 32 °C. The paste of cobalt–oleate complex is then dissolved in 130 ml of hexane and again evaporated at 32 °C. The purity and the atomic composition of the compound have been checked by quantitative energy dispersive spectrometry, EDS.

In a typical synthesis procedure of CoPt nanoalloys, platinum acetylacetonate (1.25×10^{-1} mmol), cobalt oleate (2.5×10^{-1} mmol) and 1, 2 hexadecanediol (5.6×10^{-1} mmol) are dissolved in a mixture of 10 ml of 1-octadecene, oleic acid (1.88×10^{-1} mmol) and oleylamine (1.88×10^{-1} mmol) in a three-necked round bottom flask, with magnetic stirring under nitrogen at room temperature for 1 h. In the reported polyol synthesis of CoPt, dioctyl-ether is often used as solvent but the obtained nanoparticles present crystalline defects.[21] In order to control the nanocrystallinity, we use another solvent with a higher boiling point: 1-octadecene (b.p. 317 °C). Hence the mixture is heated to the boiling point of the solvent and is refluxed for 30 min and then cooled to room temperature, giving a black dispersion, indicating the formation of the nanoparticles. The NCs are isolated by centrifuging and washed with a large excess mixture containing hexane (4%) ethanol (43%) and acetone (43%). The NCs, capped by oleic acid, can be dispersed in organic solvents such as chloroform, hexane or toluene.

B-5 Synthesis of CoPt nanoalloys by liquid–liquid phase transfer method

Cobalt–platinum NCs are made by a slightly modified synthesis of the one reported by Demortière *et al.*[19] A 168.45 mg sample of $PtCl_4$ is dissolved in 5 mL of water and 10 mL of HCl to obtain $PtCl_6^{2-}$. A 80 mL volume of toluene containing 2 g of TDAB was mixed with this platinum complex solution for 24 h. After the phase transfer, the aqueous phase is separated and discarded and we obtain the $PtCl_6(TDA)_2$ precursor. As for the platinum salt, 118.9 mg of $CoCl_2$ was used to produce the $CoCl_4(TDA)_2$ precursor. The following step of synthesis is made under nitrogen in a glove box. 10 mL of platinum organic phase and 10 mL of cobalt organic phase were added to 20 mL of toluene. After addition of octylamine (1 mL), an aqueous solution of $NaBH_4$ (378 mg, 10 mL of H_2O) is subsequently introduced into the mixture with rapid stirring. The organic phase containing the CoPt NCs was separated after 21 h of stirring. The remaining toluene in the organic phase is evaporated (until 1 mL) under vacuum in a rotavapor at 35 °C. The NCs are isolated by centrifuging and washed with a large excess ethanol and redispersed in 4 mL of toluene with 20 μL of octylamine. After one night, a final centrifugation is performed to eliminate unstable NCs or aggregates in the solution.

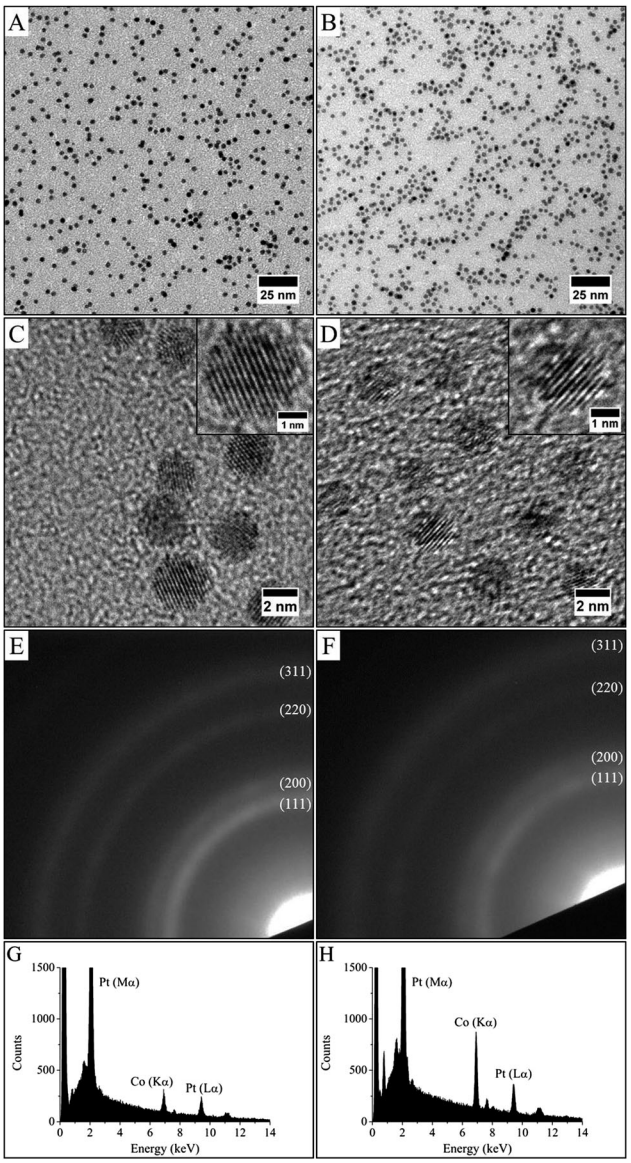

Fig. 2 TEM images (A and B), HRTEM images (C and D), electronic diffraction (E and F) and EDX analysis (G and H) of $(Co_{30}Pt_{70})_{Polyol}$ (left images) and $(Co_{50}Pt_{50})_{Polyol}$ (right images).

C. Results and discussion

C-1 Characterization of Co_xPt_{100-x} nanoalloys

Single phase methods were developed in the last decade to synthesize metallic and bimetallic NCs.[1,2] The ''polyol process'' is one of these methods. In this process, the diol or polyalcohol

(as ethylene glycol for example) is the solvent, in which the metal salts are dissolved, but which also acts as a reducing agent. This reaction is performed at high temperature (typically 100–200 °C). FePt[22] or NiPd[23] nanoalloys have been synthesized by the polyol process. As example, the use of iron acetylacetonate ($Fe(acac)_3$) and platinum acetylacetonate ($Pt(acac)_2$) in ethylene glycol or tetraethylene glycol, generates FePt NCs that show partially ordered fct structures.[24] Oleic acid or oleic amine are often used as capping agent and added directly in the chemical bath to limit the growth process. Furthermore, this high temperature process often allows to reach a better crystal quality and to avoid boron contamination often observed in monometallic nano-crystals obtained by single phase borohydride reduction.[25]

However, only few reports on the synthesis of CoPt nanoalloys by the polyol route exist, due to the difficulty to synthesize stable cobalt precursor derivate from acetylacetonate. Thus, the synthesis described here presents an original alternative using cobalt oleate and platinum acetylacetonate as precursor. Fig. 2 shows Co_xPt_{100-x} nanoalloys obtained by the polyol process with two different compositions as determined by the EDS analysis (Fig. 2G and H). They can be obtained easily by tuning the initial salt composition: $Co_{32}Pt_{68}$ nanoalloys, in average composition are obtained by mixing 1.04×10^{-1} mmol cobalt oleate to 1.25×10^{-1} mmol platinum acetylacetonate (*i.e.*, molar ratio 1.04–1.25) (Fig. 2A, C, E and G), while $Co_{52}Pt_{48}$ is obtained when the molar ratio is 2.5–1.25 (Fig. 2B, D, F and H). In both case, TEM images show well-dispersed spherical NCs (Fig. 2A and B). It can be seen that the NCs are homogeneous in size, shape and electronic contrast indicating the absence of segregation or core–shell structure.[16] A slight decrease in the average size while preserving the same polydispersity is observed for different composition of the CoPt, *i.e.* 2.9 nm with a polydispersity of 13% for $Co_{32}Pt_{68}$ and 2.5 nm with a polydispersity of 13% for $Co_{52}Pt_{48}$. Furthermore, HRTEM observations reveal crystalline nanoparticles as evidenced by clearly resolved lattice fringes (Fig. 2C and D). The selected area electron diffraction patterns (Fig. 2E and F) are similar to platinum one,[26] which indicates the formation of the face-centered-cubic (fcc) CoPt structure, which is on a chemically disordered phase A_1 (Fig. 1A) independent of the composition. Diffraction patterns appear more diffuse as the cobalt composition increases, which is consistent with an increase of the chemical disorder. This is characteristic of an alloy by substitution where platinum and cobalt atoms are randomly distributed on the platinum lattice: the higher the cobalt content, the less structural order.[19] As demonstrated previously, the combination of the SEM-EDS analysis (same composition for all the point of analysis on different film made with the same NCs) and the results obtained by TEM (homogeneous contrast and no segregation) and HR-TEM (no core–shell structure) confirms the formation of nanoalloys with the specified composition.[27] The second method used to form nanoalloys involves transfer of the metal ion from a polar phase to a non-polar phase using a transferring agent. Such an approach has been developed for synthesis of metallic nanoparticles by Brust *et al.* in the 90's.[28] This liquid–liquid phase transfer (LLPT) method, also called two-phase synthesis, has been largely used to synthesize metallic nanoparticles as silver, gold, platinum or palladium. It typically involves the transfer of the metal precursor (metallic ions) from an aqueous solution to an organic solution containing a capping molecule as alkanethiol or amine. The transfer is assisted by a phase transfer agent such as tetrakis(decyl)ammonium bromide (TDAB). Reduction of metallic precursor is then carried out by adding an aqueous solution of reducing agent (mainly $NaBH_4$) under vigorous stirring. We have reported previously the synthesis of Co_xPt_{100-x} nanoalloys by using the LLPT method.[19] In order to compare with the NCs prepared by the polyol process, nanoalloys with an average composition of the $Co_{34}Pt_{66}$ and an average size of 2.2 nm have been synthesized by the LLPT method (Fig. 3). TEM and HRTEM images confirm the formation of nanoalloys and the electron diffraction patterns are indexed to the face-centred cubic (fcc) phase (A_1 phase, Fig. 1A).

C-2 Magnetic properties of the native $Co_{30}Pt_{70}$ nanoalloys

In the following, we chose to focus our study on the particles with the composition around $Co_{30}Pt_{70}$ obtained by the two process of synthesis. For this composition a crystalline phase $L1_2$ corresponding to the fcc-ordered $CoPt_3$ is expected (see Fig. 1B).[29] The ordered $L1_2$ phase of the Co_xPt_{100-x} system shows also a high coercivity and magnetocrystalline anisotropy.

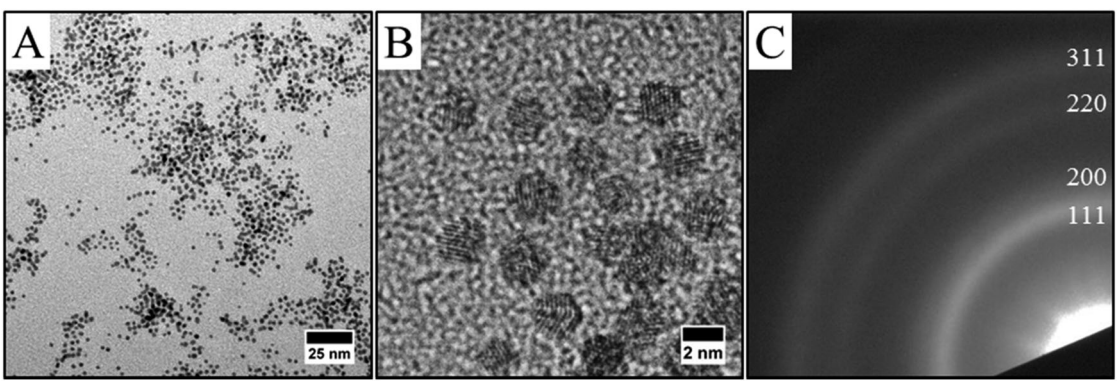

Fig. 3 TEM images (A), HRTEM images (B) and electronic diffraction (C) of $(Co_{30}Pt_{70})_{LLPT}$.

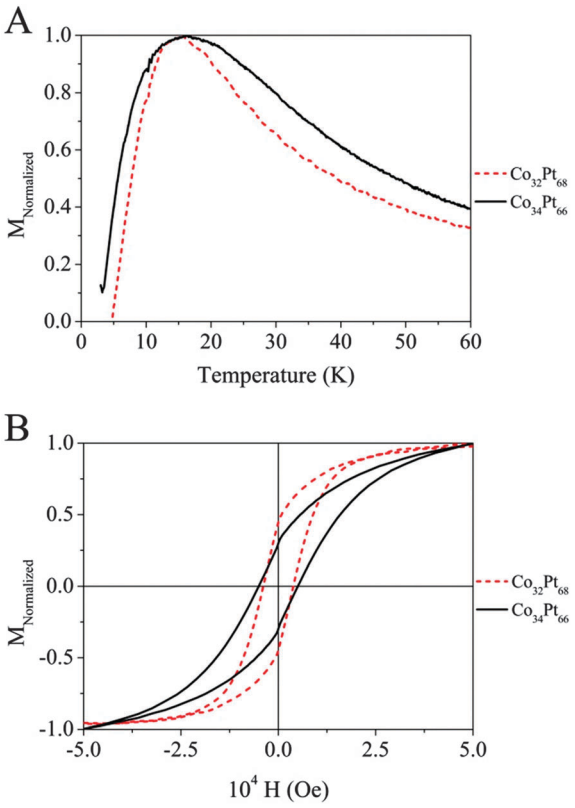

Fig. 4 (A) Temperature dependence of the magnetization in the zero-field cooled curves with applied field H = 100 Oe and (B) hysteresis loop of $(Co_{30}Pt_{70})_{Polyol}$ (dash line) and $(Co_{30}Pt_{70})_{LLPT}$ (solid line).

As for the $L1_0$ phase of CoPt, it can be obtained by annealing of the native NCs in the disordered phase. Magnetic measurements have been performed by using a VSM apparatus on the two previous samples of CoPt NCs in the A_1 crystalline phase obtained either by polyol process $(CoPt)_{Polyol}$ or by the liquid–liquid phase transfer $(CoPt)_{LLPT}$ with a composition close to $Co_{30}Pt_{70}$. The susceptibility *versus* temperature behavior is measured by a zero field cooled (ZFC)/field cooled (FC) experiment. In the ZFC measurement, the sample is cooled down to 3 K without an applied field starting from a high temperature where all the particles are in the superparamagnetic state. Afterwards, the magnetization is measured as function of the increasing temperature in an applied field of 100 Oe. In the case of an ideal system of perfectly monodisperse particles, the magnetization measured in the ZFC curve drops upon cooling from a maximum, usually defined as being the blocking temperature, T_B, to zero in a few degrees. As shown in Fig. 4A, the two ZFC curves exhibit a maximum at 15 K (Table 1). This confirms the superparamagnetic behaviour at room temperature of both samples as expected for 2–3 nm size CoPt NCs in the A_1 phase and the ferromagnetic behavior at 3 K as seen on the hysteresis loop (Fig. 4B). Indeed, from the T_B values and the average size, the particle magnetic anisotropy energy KV can be estimated by the relation $K_{eff}V = k_bT_B\ln(\tau/\tau_0) \approx 28k_bT_B$, where V is the particle volume, K_{eff} is the effective magnetic anisotropy energy per volume unit and $\tau_0 \approx 10^{-9}$–10^{-11} s.[30]

Table 1 Average diameter, polydispersity, blocking temperature (T_B), coercive field (H_C) and magnetic remanence normalized ($M_{R\text{-}Normalized}$) of $(Co_{30}Pt_{70})_{Polyol}$ and $(Co_{30}Pt_{70})_{LLPT}$

	Average diameter	Polydispersity	T_B	H_C	$M_{R\text{-}Normalized}$
$(Co_{30}Pt_{70})_{Polyol}$	2.9 nm	11%	15 K	4000 Oe	0.45
$(Co_{30}Pt_{70})_{LLPT}$	2.2 nm	13%	15 K	5000 Oe	0.30

Table 2 Distribution of crystallinity of $Co_{30}Pt_{70}$ nanoalloys depending on the synthesis route

	Monocrystals (%)	Polycrystals (%)	Undetermined (%)
$(Co_{30}Pt_{70})_{Polyol}$ (236 particles)	33	31	36
$(Co_{30}Pt_{70})_{LLPT}$ (525 particles)	21	23	56

These values take into account the volume anisotropy but also the shape and surface anisotropies. Thus the magnetic anisotropy is estimated to $K_{eff} = 5.7 \times 10^4$ J m^{-3} for 2.9 nm CoPt obtained by the polyol route and 13×10^4 J m^{-3} for the 2.2 nm CoPt obtained by the LLPT method. These values are very low compare to that of bulk $CoPt_3$ in the $L1_2$ phase ($K_a = 2 \times 10^6$ J m^{-3}) however, there is a significant difference between the two values obtained for the two sample both in the A_1 phase. It is mainly due to the surface effect contribution. This behavior is extremely important around 2 nm, where 70% of atoms are located at the surface. In fact the magnetic energy is due both to K_s, surface anisotropy and to K_v the volume anisotropy. As the size decreases the surface contribution increases. The high influence of surface atoms, which have coordination weaker than the atoms of the core, induces an important modification of the magnetic anisotropy energy.[31] It should be noticed that the shape of the ZFC curve depends on the nature of the CoPt nanoalloys. For those synthesized by the LLPT method, $CoPt_{LLPT}$, the width is significantly larger compare to those obtained by the polyol process, $CoPt_{Polyol}$. This reflects a larger distribution of the magnetic anisotropy energy (MAE). As the size distributions are similar (Table 1), this effect arises from another source. Let us consider the crystalline structure of the native $Co_{30}Pt_{70}$ nanoalloys depending on the synthetic route. Table 2 summarizes the distribution of the crystalline structure for both samples as deduced from HRTEM studies (see Fig. 2 and 3). It is clear that the crystalline distribution is larger in the case of $CoPt_{LLPT}$ than for $CoPt_{Polyol}$.

This cannot be explained by the size difference as the shape equilibrium calculation does not predict a drastic difference of stability between crystalline fcc structure and the non crystalline one as decahedron in this range of size.[32] However, the polyol process occurs at a higher temperature than the liquid–liquid phase transfer method, which is known to favor a better crystallinity. As a matter of fact, it should be noticed that the percentage of undetermined structure and polycrystals is very high for $CoPt_{LLPT}$, compare to that observed obtained by the polyol method (see Table 2). These amorphous or quasi-amorphous materials have a different magnetic anisotropy compared to the crystalline one, which could explain the larger

distribution of MAE observed Fig. 4A. This is confirmed by the hysteresis loop measured in the ferromagnetic regime at 3 K (Fig. 4B and Table 1). The coercivity at 3 K is higher for $CoPt_{LLPT}$ than for $CoPt_{Polyol}$, which is consistent with a higher magnetic anisotropy. Indeed, the coercivity increases with K_{eff}.[33] However, the reduced remanence, M_r/M_s, is lower for $CoPt_{LLPT}$. This is surprising if we consider only the anisotropy value, but could be expected if we take into account the high level of amorphous or quasi-amorphous materials, which are softer magnets compare to the ones with crystalline structure. It should also be considered that for $CoPt_{LLPT}$, some NCs are always in the superparamagnetic state even at 3 K due to the larger anisotropy distribution. This explains also the fact that magnetization at saturation is not reached even at 5 T in comparison to the $CoPt_{Polyol}$.

C-3 Ordering of the $Co_{30}Pt_{70}$ nanocrystals

Thus the fcc-CoPt NCs in the disordered A_1 phase exhibit a low magnetocrystalline anisotropy and soft magnetic properties as well. Therefore, high temperature annealing is needed (around 685 °C in the bulk phase) for the transformation from the fcc disordered A_1 to the fcc ordered $L1_2$ phase. We have demonstrated above the influence of the nanocrystallinity on the magnetic properties. Here we will consider the effect of the nanocrystallinity on the ordering by comparing the order/disorder phase transition induced by annealing of CoPt nanoalloys. This has been investigated by an *in situ* annealing, in real time and on sub-nanometer scale, using HR-TEM studies on both samples $(Co_{30}Pt_{70})_{LLPT}$ et $(Co_{30}Pt_{70})_{Polyols}$ deposited on a graphene coated TEM grid (see Experimental section). The crystallinity of the graphene film does not disturb the imaging of the nanoparticles due to the large difference in the atomic number and mass/thickness of the nanoparticles (Z_{Co} = 27, Z_{Pt} = 78) and the thin carbon layer (Z_C = 6) below them.

Fig. 5 shows a typical structural evolution of the $(Co_{30}Pt_{70})_{Polyols}$ NCs during the *in situ* annealing process. It can be seen that, in comparison to the native NCs, there is a slight and continuous increase of the average size with the annealing temperature (Table 3). This has been already observed during annealing process of CoPt and attributed to an Ostwald ripening to the benefit of larger nanoparticles.[34] HR-TEM patterns at 300 °C show lattices fringes of the NCs, characteristics of the disordered A_1 phase with a lattice spacing equal to 2.14 Å (Fig. 5A). This is confirmed by the power spectrum, where only one pair of reflection corresponding to the (111) plane is observed. The deduced lattice parameter is equal to 3.70 Å, which is consistent with an A_1 fcc structure. In fact no variation of the lattice parameters is observed compared to the value obtained at room temperature (Fig. 2C). Upon rising the temperature to 420 °C, (Fig. 5B), a drastic structural evolution is observed: some NCs exhibit different fringe patterns characteristics from the ordered fcc $L1_2$ phase with a lattice parameters of 3.85 Å as deduced from power spectrum (Fig. 5B3 and Table 4). Indeed the corresponding power spectrum clearly shows characteristics reflections corresponding to the (001) plane, which confirm the formation at low temperature of ordered $CoPt_3$ nanoalloys. It should be noticed that no sintering effect is observed and the NCs still remain isolated on the graphene support. In fact, on the particles prepared by the polyol process at high temperatures graphitic shells can be observed (Fig. 5). These shells are very thin and might be due to the capping agent transforming during annealing, which actually protects the particles against coalescence.

Table 3 Mean diameter and polydispersity of $(Co_{30}Pt_{70})_{Polyol}$ nanoalloys at different temperature of the annealing process

	25 °C	300 °C	420 °C	550 °C	680 °C
Mean diameter	2.9 nm	2.7 nm	3.0 nm	3.3 nm	3.2 nm
Polydispersity	11%	12%	17%	15%	12%

Further increase of the temperature induces the ordering of more and more NCs (Fig. 6 and Table 3) as well as a continuous increase of the lattice parameters. This isotropic expansion of the lattice parameter is characteristic of the ordering of $CoPt_3$ indicating a homogeneous order–disorder transformation.[34] The bulk value is equal to 3.9 Å,[35] reached in our case at 680 °C, which indicates that the ordering is total.

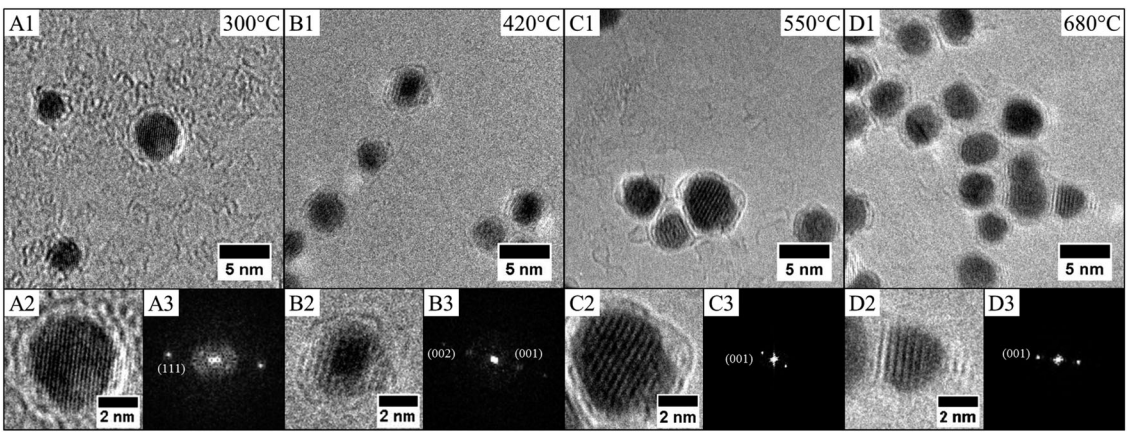

Fig. 5 HRTEM images of $(Co_{30}Pt_{70})_{Polyol}$ at various annealing temperatures: (A) 300 °C; (B) 420 °C; (C): 550 °C and (D) 680 °C. For each temperature, HRTEM images of one nanoparticle (A2, B2, C2, D2) and the associated FFT (A3, B3, C3, D3).

Table 4 Structural evolution during the annealing of $(Co_{30}Pt_{70})$ obtained by polyol process. Only nanoparticles with visible atomic planes included in the percentage of disordered nanoparticles (A_1) and ordered nanoparticles ($L1_2$). The ratio ($L1_2/A_1$) is given for each temperature. The lattice parameters are deduced from the power spectra shown on Fig. 5

Temperature	300 °C	420 °C	550 °C	680 °C
Number of nanoparticles studied with observable atomic planes	161	161	191	77
Lattice parameters (Å)	3.70	3.85	3.86	3.90
% A1	100	83	59	43
% $L1_2$	0	17	41	57
$L1_2$/A1	0	0.20	0.69	1.33

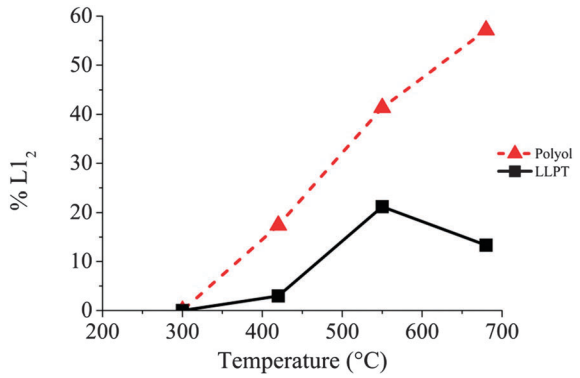

Fig. 6 Evolution of ordering with temperature during the annealing process.

Table 4 shows also the statistical evolution of the ordering of the NCs. At 680 °C, 57% of the observed NCs are in the ordered $L1_2$ structure. In fact there is a linear evolution of this percentage with the annealing temperature as shown of Fig. 6 in relation with the evolution of the lattice parameters. This indicates a continuous and monotonic transition from the ordered to the disordered fcc structure of $CoPt_3$. Indeed, this low temperature transition is surprising. Even if it has been reported, and calculated, a decrease of the transition temperature in the Co_xPt_{1-x} phase diagram in case of NCs compared to bulk materials,[32,36] this value is close to 180 °C below the bulk value (around 760 °C[29]), for 3 nm in size NCs. Here we observe significantly larger decrease of 350 °C of the order/disorder transition.

Fig. 7 and Table 5 show the same experiment with $Co_{30}Pt_{70}$ NCs prepared by the LLPT method. The behavior of these NCs strongly differs from both structural and ordering point of view.

Similarly to the previous case of NCs prepared by the polyol process, no ordering is observed for the LLPT prepared NCs, upon increasing the temperature to 300 °C. For the NCs prepared by the LLPT process, however, significant coalescence occurs, even if isolated NCs are still present on the graphene support film. This effect probably arises from the nature of the passivating agent on the CoPt surfaces, depending on the chemical route. Indeed, alkylamines are used in this soft synthetic method where as $(Co_xPt_{100-x})_{Polyol}$ are coated by carboxylate derivatives (see Experimental methods). In case of $(Co_xPt_{100-x})_{LLPT}$, this is due to the growth process taking place at room temperature, which is totally inhibited if chemically bond agents are used as a capping agent.[37] As a result, their protection is not strong enough to avoid a coalescence process. However, operating *in situ* on deposited NCs on the TEM grid limit the progression of this process during the annealing and allows us to study the ordering of $(Co_{30}Pt_{70})_{LLPT}$. From a crystalline point of view, no transition is observed at 300 °C independent of the size of the NCs. The lattice parameter also corresponds to the (111) plane of the A_1 disordered fcc structure (Table 5). At 400 °C only a very small part of NCs undergo a structural evolution towards the $L1_2$ fcc ordered phase: 3% of the observed NCs when it was 17% for the $(Co_{30}Pt_{70})_{Polyols}$. This finding cannot be explained only by a size effect as the corresponding transition is not observed for the smallest NCs. Further increase of the annealing temperature yields

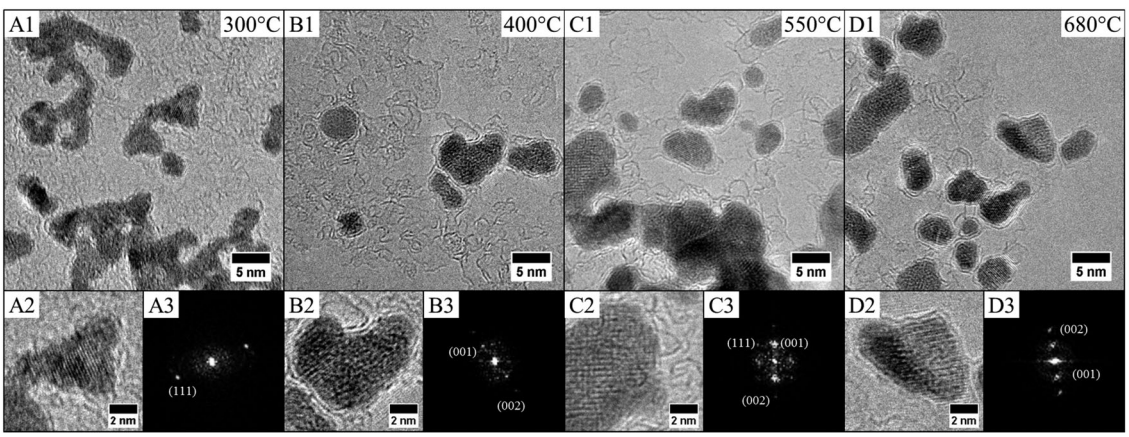

Fig. 7 HRTEM images of $(Co_{30}Pt_{70})_{LLPT}$ at various annealing temperatures: (A) 300 °C; (B) 400 °C; (C): 550 °C and (D) 680 °C. For each temperature, HRTEM images of one nanoparticle (A2, B2, C2, D2) and the associated FFT (A3, B3, C3, D3).

Table 5 Structural evolution during the annealing of ($Co_{30}Pt_{70}$) obtained by LLPT process. Only nanoparticles with visible atomic planes were taken in count in the percentage of disordered nanoparticles (A_1) and ordered nanoparticles ($L1_2$). The ratio ($L1_2$/A1) is given for each temperature. The lattice parameters are deduced from the power spectra shown on Fig. 6

Temperature	300 °C	400 °C	550 °C	680 °C
Number of nanoparticles studied with observable atomic planes	51	101	99	30
Lattices parameters (Å)	3.91	3.60	3.84	3.63
% A1	100	97	79	87
% $L1_2$	0	3	21	13
$L1_2$/A1	0	0.03	0.27	0.15

an increase of the number of NCs in the $L1_2$ phase, but their proportion is always significantly lower than for the $(Co_{30}Pt_{70})_{Polyols}$. (Fig. 6 and Table 5). At 680 °C only 15% of the observed NCs present a $L1_2$ structure.

The established strong difference of chemical ordering depending on the chemical route of preparation of the NCs can be understood if we take into account the difference of crystallinity reported above. It has been reported in similar annealing process of CoPt nanoalloys that the transformation of A_1 to $L1_0$ (or $L1_2$) is a multi-step process.[34] There is first a transition from polycrystalline, or non-crystalline phase as decahedron, to a fcc truncated octahedron structure. Simultaneously, the NCs size increases and their shape becomes more and more isotropic. Further increase of the temperature induces the chemical ordering of the NCs keeping a fcc octahedron structure. Indeed it has been reported that the non-crystallinity of the NCs is a limiting factor to achieve the chemical order. Furthermore coalescence of the NCs during the annealing process often yield to high angle grain boundaries, which also prevent or slow down the chemical ordering and the homogeneous crystalline transition as numerous energetic barriers should be overcome to achieve the correct crystalline structure.[15] Thus chemical ordering can only be reached at higher temperature. In our case, on one hand $(CoPt)_{LLPT}$ present an important part of non crystalline or amorphous structure (Table 2), on the other hand the passivating agent is not strong enough to prevent the coalescence conversely to the case of $(CoPt)_{Polyol}$. As a result the chemical ordering appears at lower temperature and on larger scale for CoPt nanoalloys made by the polyol process compared to similar NCs synthesized by the LLPT process. This is probably reinforced by the fact that the polyol process is a high temperature synthetic method, which favors a better crystallinity of the NCs. Thus the first step of the order transition considered above is limited or inexistent. Moreover, this assumption is further confirmed if we consider the chemical ordering of $Co_{50}Pt_{50}$ synthesized by the polyol process (Fig. 8). Again $Co_{50}Pt_{50}$ NCs present mainly a disordered fcc A_1 crystalline structure, with a truncated octahedron shape, and only few NCs with non-crystalline structure are observed. As a consequence, similar behavior as reported above for $Co_{30}Pt_{70}$, is observed during the *in situ* annealing in the TEM. For a 50–50 composition the ordered structure, as deduced from the phase diagram, is the tetragonal fct $L1_0$ phase (see Fig. 1). It can be obtained by annealing because chemical synthesis only produce the disordered A_1 structure. The *in situ* TEM experiments with these NCs show slight coarsening due to the Ostwald ripening of the NCs as their size increase from 2.5 to 3.0 nm but without coalescence. Furthermore, ordering occurs also at low temperature (420 °C) and the nanoparticles retain their ordered $L1_0$ structure after cooling down to low temperature as observed on Fig. 8E and F. Our previous study on NCs synthesized by the LLPT method with same size, but passivated also by alkylamine chains showed a huge coalescence and a chemical ordering only above 500 °C.[16] Again, we observe the beginning of chemical ordering at lower temperature for $(CoPt)_{Polyol}$ than for $(CoPt)_{LLPT}$ independent of the composition.

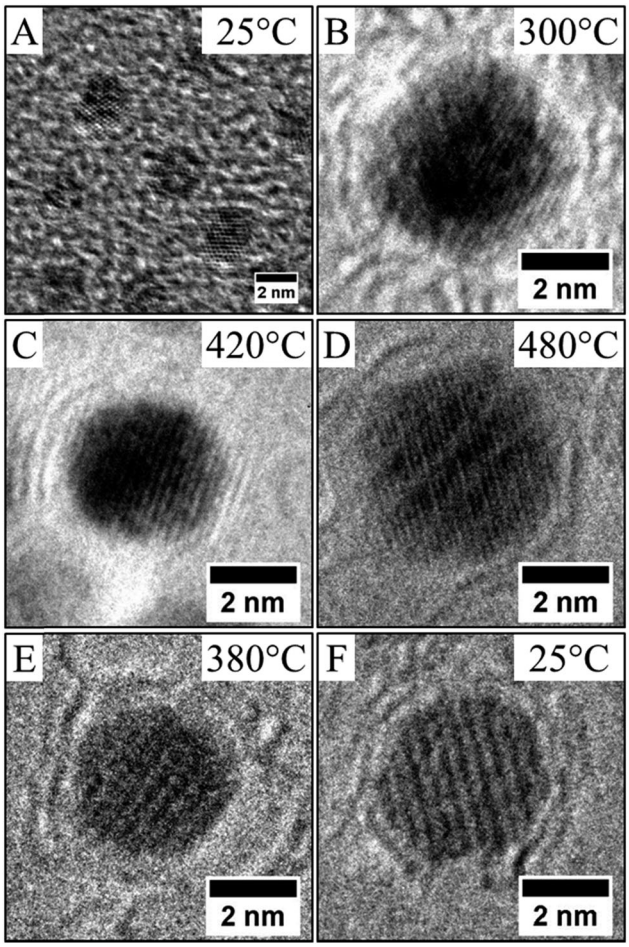

Fig. 8 HRTEM images of $(Co_{50}Pt_{50})_{Polyol}$ during annealing treatment: (A) room temperature (RT), (B) 300 °C, (C) 420 °C on the increasing part of the annealing and (D) 480 °C, (E) 380 °C and (F) RT on the decreasing part of the annealing.

D. Conclusion

We have reported here a new synthesis of bimetallic Co_xPt_{100-x} NCs by the polyol process, allowing substantial control over the composition of these nanoalloys. Structural analysis performed by TEM and HR-TEM show that, compared to conventional soft chemical approach, the nanocrystallinity of these nanoalloys strongly differs as fcc structure is mainly observed even for very low size. The decrease of the crystalline polydispersity induces a decrease of the magnetic anisotropy energy distribution as observed by magnetic measurement. Furthermore, the order/disorder transition induced by annealing and observed *in situ* by HR-TEM studies, clearly demonstrates a decrease of the chemical ordering temperature compared to the bulk value but also to NCs obtained by soft chemistry. The absence of coalescence during the annealing allows us to develop a new approach to obtain periodic 2D self-assembly of chemically ordered nanoalloys. Hence it is clearly demonstrated the importance of the chemical preparation route on the crystallinity of the NCs. This strongly influences the physical and chemical properties of the NCs.

Acknowledgements

This work was supported by the French ANR within the program ''Nanocrisnet'' under Contract ANR-11-BS10-018 and by the LabEx MiChem part of French state funds managed by the ANR within the ''Investissements d'Avenir'' program under reference ANR-11-IDEX-0004-02. This research has been carried out in part at the Center for Functional Nanomaterials, Brookhaven National Laboratory, which is supported by the U.S. Department of Energy, Office of Basic Energy Sciences, under Contract No. DE-SC0012704. Thanks are also due to the ''Service commun de microscopie de l'UFR de Chimie de l'UPMC'' and to S. Casale for their help in the TEM characterization of the nanocrystals.

References

1 *Nanoalloys*, ed. D. alloyeau, C. Mottet and C. Ricolleau, Springer, 2012.
2 *Nanoalloys: From Fundamentals to Emergent Applications*, ed. F. Calvo, Elsevier, 2013.
3 R. Ferrando, J. Jellineck and R. L. Johnston, *Chem. Rev.*, 2008, **108**, 845.
4 Q. Zhang, J. Xie, Y. Yu and J. Y. Lee, *Nanoscale*, 2010, **2**, 1962.
5 M. L. Plumer, J. Van Ek and D. Weller, *The Physics of Ultra-High-Density Magnetic Recording*, Springer, 2001.
6 D. Weller and A. Moser, *IEEE Trans. Magn.*, 1999, **35**, 4423.
7 S. Sun, C. B. Murray and D. Weller, *et al.*, *Science*, 2000, **287**, 1989.
8 P. Gambardella, S. Rusponi, M. Veronese, S. S. Dhesi, C. Grazioli, A. Dallmeyer, I. Cabria, R. Zeller, P. H. Dederichs, K. Kern, C. Carbone and H. Brune, *Science*, 2003, **300**, 1130.
9 X. Sun, Z. Y. Jia, Y. H. Huang, J. W. Harrell, D. E. Nikles, K. Sun and L. M. Wang, *J. Appl. Phys.*, 2004, **95**, 6747.
10 T. J. Klemmer, N. Shukla, C. Liu, X. W. Wu, E. B. Svedberg, O. Mryasov, R. W. Chantrell and D. Weller, *Appl. Phys. Lett.*, 2002, **81**, 2220.
11 E. E. Carpenter, J. A. Sims, J. A. Wienmann, W. L. Zhou and C. J. O'Connor, *J. Appl. Phys.*, 2000, **87**, 5615.
12 Y. Huang, Y. Zhang, G. C. Hadjipanayis, A. Simopoulos and D. Weller, *IEEE Trans. Magn.*, 2002, **38**, 2604.
13 G. W. D. Spratt, P. R. Bissell, R. W. Chantrell and E. P. Wohlfarth, *J. Magn. Magn. Mater.*, 1998, **75**, 309.
14 H. Zeng, S. Sun, T. S. Vedantam, P. Liu, Z. Dai and Z. L. Wang, *Appl. Phys. Lett.*, 2002, **80**, 2583.
15 T. J. Klemer, C. Liu, N. Shukla, X. W. Wu, D. Weller, M. Tanase, D. E. Laughlin and W. A. Soffa, *J. Magn. Magn. Mater.*, 2003, **266**, 79.
16 A. Demortière and C. Petit, *J. Appl. Phys.*, 2011, **109**, 084344.
17 M. Chen and D. E. Nikles, *J. Appl. Phys.*, 2002, **91**, 8477–8479.
18 F. Somodi, Z. Peng, A. B. Getsoian and A. T. Bell, *J. Phys. Chem. C*, 2011, **115**, 19084.
19 A. Demortière and C. Petit, *Langmuir*, 2007, **23**, 8575.
20 A. T. Ngo, J. Richardi and M. P. Pileni, *Phys. Chem. Chem. Phys.*, 2013, **15**, 10666.
21 B. Hyun, J. H. Wu, H. L. Liu, S. P. Ko, J. S. Ju and Y. K. Kim, *Colloids Surf., A*, 2008, **313**, 250.
22 S. Sun, *Adv. Mater.*, 2006, **18**, 393.
23 F. Ai; A. Yao, W. Huang, D. Wang and X. Zhang, *Physica E*, 2010, **42**, 1281.
24 L. C. Varanda and M. Jafelici, Jr., *J. Am. Chem. Soc.*, 2006, **128**, 11062.
25 J. Park, J. Joo, S. G. Kwon, Y. Jang and T. Hyeon, *Angew. Chem.*, 2007, **46**, 4630.
26 K. Wikander, C. Petit, K. Holmberg and M. P. Pileni, *Langmuir*, 2006, **22**, 4863.
27 A. Demortière, R. Losno, C. Petit and J.-P. Quisefit, *Anal. Bioanal. Chem.*, 2010, **397**, 1485.
28 M. Brust, M. Walker, D. Bethell, D. J. Schiffrin and R. Whyman, *J. Chem. Soc., Chem. Commun.*, 1994, 801.
29 C. Leroux, A. Loiseau, D. Broddin and G. Vantendeloo, *Philos. Mag. B*, 1991, **64**, 57.
30 E. Tronc, *Il Nuovo Cimento D*, 1996, **18**, 163.
31 A. Demortière, S. Buathong, B. P. Pichon, P. Panissod, D. Guillon, S. Bégin-Colin and B. Donnio, *Small*, 2010, **6**, 1341.
32 G. Rossi, R. Ferrando and C. Mottet, *Faraday Discuss.*, 2008, **138**, 193.
33 L. Weil, *J. Phys. Radium*, 1951, **12**, 437.
34 P. Andreazza, C. Mottet, C. Andreazza-Vignolle, J. Penuelas, H. C. N. Tolentino, M. De Santis, R. Felici and N. Bouet, *Phys. Rev. B: Condens. Matter Mater. Phys.*, 2010, **82**, 155453.
35 S. U. Jen, *J. Alloys Compd.*, 1996, **234**, 231.
36 D. Alloyeau, C. Ricolleau, C. Mottet, T. Oikawa, C. Langlois, Y. Le Bouar, N. Braidy and A. Loiseau, *Nat. Mater.*, 2009, **8**, 940.
37 C. Salzemann and C. Petit, *Langmuir*, 2012, **28**, 4835.